Diameter dependence of mechanical, electronic, and structural properties of InAs and InP nanowires: A first-principles study

Cláudia L. dos Santos and Paulo Piquini
Departamento de Fisica, Universidade Federal de Santa Maria, 97105-900 Santa Maria, RS, Brazil
(Received 10 July 2009; revised manuscript received 22 September 2009; published 5 February 2010)

Semiconductor nanowires (NWs) have ideal morphologies to act as active parts and connections in nanodevices since they naturally restrict the conduction channels and periodicity to one dimension. The advantages from the reduced spatial dimension can be greatly enhanced by wisely selecting the materials composing the NWs, through the knowledge of the properties of their bulk counterparts. NW's properties can still be tailored by managing (i) internal or intrinsic characteristics as diameters, growth directions, structural phases, and the faceting or saturation of surfaces, and/or (ii) external or extrinsic influences as applied electric, magnetic, thermal, and mechanical fields. Bulk InAs has one of the lowest electron effective-masses among binary III-V semiconducting materials while bulk InP shows excellent optical properties, which make InAs and InP NWs candidates for optoelectronic materials. In this work, we use first-principles calculations to study the structural, electronic, and mechanical properties of [111] zinc-blende InAs and InP NWs as a function of diameter (ranging from 0.5 to 2.0 nm). The influence of external mechanical stress on the electronic properties is also analyzed. The axial lattice constants of the NWs are seen to decrease with decreasing diameter, as a consequence of a shorter surface lattice constant of the NWs, as compared to their bulk values. The Young's modulus of both InAs and InP NWs is determined to decrease while the Poisson's ratio to increase with decreasing diameters, with deviations from the bulk Young's modulus estimated to occur for NWs with diameters lower than 15 nm. The increase in the band-gaps with decreasing diameters is seen to be slower than the expected from simple quantum-mechanical models ($1/D^2$, where D is the diameter), mainly for the smallest (<1.0 nm) diameters. The electron effective-masses are seen to increase with decreasing diameters, due to a k-dependent energy shift of the conduction-band minimum. The calculated work functions for both NWs show a decrease with decreasing diameters. The change in the NWs' band-edge eigenvalues with axial strain is calculated and the band-gap deformation potentials are determined and shown to change in signal within the range of studied diameters. The influence of the mechanical strain on the electronic bands is analyzed in terms of electronic charge decompositions in directions parallel and perpendicular to the NWs' axes. Direct to indirect band-gap transitions are observed for compressive strains in very thin NWs. The hole effective-mass is seen to be lower than the corresponding electron effective-mass for the studied NWs.

DOI: 10.1103/PhysRevB.81.075408 PACS number(s): 62.23.Hj, 71.15.Mb, 73.63.Nm

I. INTRODUCTION

Semiconductors nanowires (NWs) have great potential for technological applications, such as the field-effect transistors,[1,2] logical gates,[3] biological sensors,[4] lasers,[5] light-emitting diodes,[2] nanoscale interconnects, and active components of optoelectronic devices and nanoelectromechanical systems.[6–8]

NWs are quasi-one-dimensional systems with a small cross-section area and a large surface/volume ratio, with charge carriers confined in two directions. Differently from single-wall nanotubes, NWs can be built from a large variety of materials. For specific applications, the choice of the NW system is guided by the knowledge about the performance of the corresponding bulk material. Thus, bulk materials which show outstanding results in, e.g., electronic applications, will naturally be candidates for NW electronic devices. InAs is known to have one of the lowest electron effective-masses among the III-V materials,[9] small band-gap, and a Fermi-level pinning at the conduction-band which leads to almost ideal ohmic contacts. Thus, InAs NWs are expected to show excellent performance in electronic applications. On the other hand, bulk InP has a direct band-gap and high luminescence quantum yield, which turn InP NWs a natural choice for optoelectronic devices.

Several experimental[10–25] and theoretical[26–31] studies of InAs and InP NWs have been performed. Thelander *et al.*[10] studied the electronic transport on InAs NWs and InAs/InP NW heterostructures, and showed strong confinement effects and depletion of charge carriers for wires with diameters less than 30 nm. Information about doping and surface states concentrations were obtained by studying the capacitance of arrays of wrapped-gate InAs NWs.[11] Sørensen *et al.*[12] observed ambipolar conduction in Be-doped InAs NWs without surface modification. Studies of the diameter dependence on the transport coefficients[13] and electron mobility[14] of InAs NWs have been performed and a reduction in the effective mobility with decreasing diameter was observed. Successful growth of InAs NWs in modified (111) Si substrate has been achieved by Tomioka *et al.*[16] The influence of surface passivation on the transport properties of InAs NWs were determined by Hang *et al.*,[17] which showed that electron mobility in passivated devices is superior to the unpassivate ones. Photoluminescence spectra has been used to distinguish zinc-blende and wurtzite InP NWs.[18,19] An increase in the photoluminescence intensity in oxide-passivated InP NWs has been reported by van Vugt *et al.*[20] It was shown that Zn-doped InP NWs show a preference for zinc-blende instead of wurtzite structures.[21] Cornet *et al.*[22] showed that there is a minimum length of 300 nm for the onset of stacking faults in

 ©2010 The American Physical Society

InP NWs. Gudiksen *et al.*[24] studied the size dependence of photoluminescence in InP NWs with diameters ranging from 10 to 50 nm, and showed a systematic shift of the emission maxima for wires with diameter lower than 20 nm. Moewe *et al.*[25] showed that InP NWs, grown on lattice-mismatched GaAs, can have crystalline wurtzite or zinc-blende phases, depending on the size of the catalytic Au nanoparticles. Galicka *et al.*[26] performed first-principles calculations to study the energetic stability of wurtzite and zinc-blende InAs and GaAs NWs for different diameters and growth directions, showing that [0001] wurtzite wires have lower formation energies for diameters less than 50 nm while zinc-blende and wurtzite NWs have similar formation energies for larger diameters. Persson and Xu[27] used a tight-binding approach to study wave functions and band structures of InAs and InP NWs with rectangular and square cross sections, and found parabolic-like conduction-band structures. Schmidt *et al.*[28] performed *ab initio* pseudopotential calculations to study the scaling with diameter of the band-gap of InP NWs and found deviations of the $1/d^2$ behavior for diameters d lower than 2 nm. Moreira *et al.*[29] studied the effects OH surface passivation on InP NWs, and showed the presence of localized states near the band-edges. Akiyama *et al.*[30] investigated the stability of InP NWs and showed that the wurtzite structure is stabilized due to contributions of surface dangling bonds for small (<12 nm) diameters. Alemany *et al.*[31] showed, through first-principles calculations, that the binding energy of acceptor states in InP NWs vary from its bulk value up to 0.2 eV in thinner NWs due to quantum confinement.

Compared to the number of experimental and theoretical studies about the electronic, structural, and optical properties of NWs, few works involving the mechanical properties of these nanostructures have been performed. However, the possible applicability of these nanomaterials in nanoelectromechanical systems and the great probability of deformations in their structures when integrated in functional devices turn it necessary to know how the properties of these nanomaterials vary when they are strained.

It is known that the strain has an important role in the electronic and optical properties of NWs. Zhang *et al.*[6] showed that uniaxial strain in ⟨111⟩ Ge nanowires leads to direct band-gap materials while Zhang *et al.*[32] found a direct-indirect band-gap transition with uniaxial compression in ultrathin ZnO NWs. Lyons *et al.*[33] reported that strained Si nanowires show a shift in the photoluminescence spectra, induced by changes in their band structures, due the strain. Recent theoretical studies in Si NWs along the [112] direction,[34,35] have indicated a possible change from indirect band-gap in the ultrathin diameters regime to quasi-direct band-gap in thicker wires. In addition, a compressive stress applied along the wire axis can enhance the quasi-direct band-gap feature in these systems. The strain has also been used to increase the mobility in planar Si metal-oxide-semiconductor-field-effect transistors.[36] Strain effects in optical band-gaps of GaN nanowires were observed.[37] Some tight-binding calculations have been performed to study the strain effects in GaAs NWs (Ref. 38) and theoretical studies have been done in strained carbon nanotubes.[39,40]

Another fundamental question concerning the behavior of nanomaterials is the size dependence of their mechanical properties. Many studies have been done for the mechanical properties ZnO nanowires and no agreement has been achieved on how the elastic moduli of these systems depend on their geometry and sizes. Experimental measurements by Bai *et al.*[41] and Ni and Li[42] indicated that the elastic modulus of ZnO nanobelts is lower than that for the bulk material. In contrast, Chen *et al.*[43] reported that the elastic modulus for ZnO NWs with diameters ranging from 17 to 550 nm is higher than that of bulk material (140 GPa) and increase with the decreasing of the nanowire diameter. The same trend was also observed by Wang *et al.*,[44] who studied the structural, mechanical, and electronic properties of ultrathin ZnO nanowires (1–2 nm) along the [0001] direction. Leu *et al.*[45] showed, using a first-principles approach, that the Young's modulus and the Poisson's ratio of [110] and [111] Si NWs, with diameter ranging from 0.7 to 2.6 nm, decrease with decreasing diameter. Experimentally, the Young's modulus of Ag and Pb NWs have been found to increase with decreasing diameters[46] while investigations on Au NWs point that their elastic moduli do not depend on diameters.[47] Theoretical models have been proposed to explain the size dependence of the elastic modulus of nanostructures. Most of these models use the linear elasticity theory and are based on the surface-free energy and its first two derivatives, i.e., the surface stress and the surface elastic constants.[43,46,48–50] Usually in these approaches, the nanostructure is artificially divided in two distinct regions: (i) a core, with the elastic modulus of the bulk material and (ii) a surface, with a surface modulus, which is related to the surface effects. Liang *et al.*[51] using the embedded-atom method, explains the size dependence of the Young's modulus of Cu NWs as due to a nonlinear behavior of the NW core. To our knowledge, no studies on mechanical properties of InAs and InP NWs have been performed.

In this work we present the results of first-principles calculations of mechanical, electronic, and structural properties of [111] zinc-blende InAs and InP nanowires. Details of the employed methodology are shown in Sec. II. The results of diameter dependence of the NWs' mechanical and structural properties are presented in Sec. III A. The size and stress dependences of the electronic properties are showed in Secs. III B 1 and III B 2, respectively. Our conclusions are summarized in Sec. IV.

II. METHODOLOGY

The calculations were performed with the Vienna *ab initio* package simulation code (VASP),[52] using the density-functional theory (DFT) within the local-density approximation (LDA) to the exchange-correlation potential,[53,54] and the projector-augmented wave method (PAW).[55] The Kohn-Sham single-particle wave functions are represented by plane-wave expansions with a cutoff of 314 eV for InAs and 405 eV for InP.

In order to check the accuracy of the employed methodology and to establish limiting values for the size dependence of the NW properties, we calculated the electronic, structural, and mechanical properties of bulk zinc-blende InAs and InP materials. For these bulk calculations, a sampling of the Brillouin-zone with ten special k points was

TABLE I. Calculated equilibrium lattice constants, a_0, Bulk modulus, B_0, and band gaps, E_g, for bulk zinc-blende InAs and InP. The results in parentheses are taken from Ref. 58.

	a_0 (Å)	B_0 (GPa)	E_g (eV)
InAs	6.059 (6.058)	60.2 (57.9)	−0.34 (0.418)
InP	5.879 (5.869)	71.3 (72.4)	0.52 (1.424)

used, according to the Monkhorst-Pack scheme.[56] Total energy calculations for several values of the lattice constant were performed, and a fit to the Murnaghan equation of state[57] was done in order to obtain the equilibrium lattice constants as well as the Bulk moduli of InAs and InP. Apart from the band-gap values, which are underestimated in DFT/LDA calculations, our results are in good agreement with literature,[58] as shown in Table I.

The mechanical properties of bulk InAs and InP materials were studied along the [001] and [111] directions. Starting from the equilibrium configurations, total energy calculations have been performed for unit cells strained from −4% to +4% of the lattice constants along the appropriate directions. For each strained bulk calculation, an optimization of the unit cell dimensions along directions perpendicular to the applied strain was performed. The Young's moduli, Y_0, and Poisson's ratios, ν_0, of these systems have been determined according to the following equations:

$$Y = \frac{1}{V}\left(\frac{d^2E}{d\epsilon^2}\right)_{\epsilon=0}, \tag{1}$$

$$\frac{\Delta V}{V} = (1-2\nu)\epsilon, \tag{2}$$

where E is the total energy, ϵ is the strain, and V is the equilibrium volume. The results for the bulk Young's moduli and Poisson's ratios at [001] and [111] directions, shown in Table II, are in good agreement with literature.[59,60]

We studied zinc-blende [111] InAs and InP nanowires with diameters of 0.5, 1.0, 1.5, and 2 nm, approximately. Figure 1 shows the cross sections of the studied NWs. All NWs present six {110} planes, forming hexagonal cross sections, with the dangling bonds at the surfaces saturated with pseudohydrogen atoms.[61] The introduction of saturating

TABLE II. Calculated Young's moduli (Y_0) and Poisson's ratios (ν_0) for bulk zinc-blende InAs and InP, along [001] and [111] directions. Experimental results for InAs, in parentheses, are taken from Ref. 59 and for InP from Ref. 60.

	Y_0 (GPa)		ν_0	
	[001]	[111]	[001]	[111]
InAs	48.1 (50.0)	91.2	0.369 (0.36)	0.252
InP	56.0 (61.1)	106.4 (112.7)	0.368 (0.357)	0.255 (0.236)

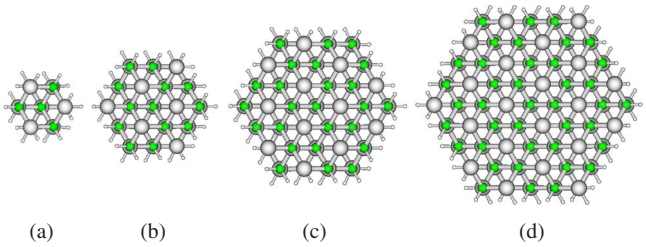

FIG. 1. (Color online) Representative cross sections of the studied InAs and InP NWs with diameters of ≈ (a) 0.5, (b) 1.0, (c) 1.5, and (d) 2.0 nm.

pseudohydrogen atoms requires an increase in the cutoff of plane-wave expansion from 314 to 375 eV in the case of the InAs NWs. We used tetragonal unit cells with the minimal size along the NW axis and a vacuum layer of 8 Å in the directions perpendicular to NW axis. This construction avoids the interaction between NW images in neighboring cells. The numbers of atoms in the unit cells are 14, 38, 74, and 122 cation plus anion atoms (excluding the pseudo-H atoms) for the four studied NW diameters. The sampling of the NWs' one-dimensional Brillouin-zones was performed by using two k points. A convergence in the total energy within 5 meV was obtained. We optimize the geometry of the InAs and InP NWs until the forces are lower than 0.03 eV/Å.

There is no unique definition for the NW diameters. Here, we define the NW diameters as those of the thinnest cylinders that contain the NWs excluding the saturation layer. The volume of the NWs are calculated as those of regular hexagonal prisms. It is important to stress at this point that the numerical values obtained for the NW properties are dependent on the way the diameter is defined. However, the trends in these properties are independent of this specific choice of the NW diameters.

III. RESULTS AND DISCUSSION

A. Structural and mechanical properties

When the chemical bonds are broken to the formation of a surface layer in a bulk material, two processes can occur, namely, relaxation and reconstruction. The environment of the surface atoms differ significantly from the bulk atoms. Even in cases where surface passivation is taking into account, there are differences in the bond strengths at the surface. These differences of bond strengths possibly lead to surface lattice constants that are different from those of the bulk material. It introduces compressive or tensile stress between the surface and bulk atoms, resulting in equilibrium lattice constant for the entire system that will be dependent on the surface/volume ratio. As this ratio increases, as in the cases for small diameter NWs, the resulting lattice constant will be the one which minimizes the stress in the system.

For the InAs and InP NWs studied here, only relaxations of the surface atoms can occur since we are passivating the dangling bonds at the surface. Figure 2 shows the variation in the lattice constant for the [111] InAs and InP NWs as a function of the NW diameter. It can be seen from this figure

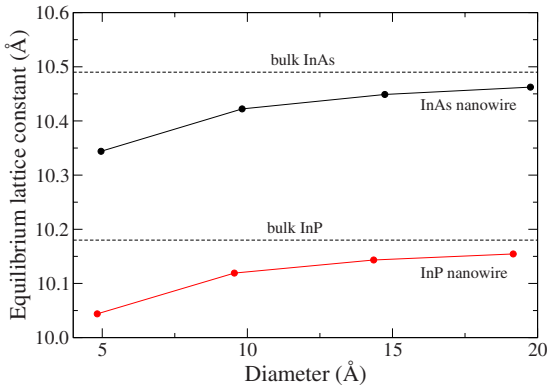

FIG. 2. (Color online) Calculated variation in the equilibrium lattice constant of the InAs and InP NWs as a function of the NW diameters. The dashed horizontal lines represent the bulk equilibrium lattice constants.

that the lattice parameter of the NWs turn shorter as the diameter decreases and deviations from the bulk value, although small, already occurs for NWs with diameters around 20 Å. These deviations in the NWs' lattice constants show that the surface lattice constant is certainly smaller than that for the bulk materials, i.e., the surfaces are under tensile stress.

The Young's modulus for the [111] InAs and InP nanowires, Y_{NW}, have been determined through a quadratic fit to Eq. (1) by calculating the total energy of the NWs at eight different strain values, corresponding to deviations from −4% to +4% of the axial equilibrium lattice constants. Figures 3(a) and 3(b) show the deviations of the InAs and InP NWs Young's moduli from the respective bulk values, ΔY. The Young's moduli of the NWs clearly decrease as the diameter decreases. This occurs because the atoms at the surface and in the core of the NWs are subject to different chemical environments and will respond differently to external stresses. Thus, the calculated effective Young's modulus for these small diameter NWs will be the result from combined core and surface contributions. In order to quantify these two distinct contributions, one should have a way to separate the atoms in the NWs in surface and core regions. Since there is no unique way to define a surface region, we

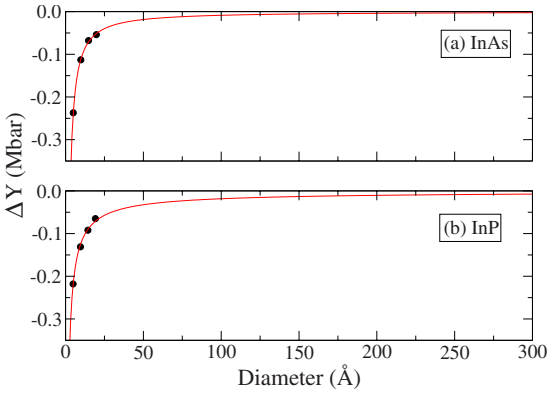

FIG. 3. (Color online) Calculated variation in the Young's modulus for the [111] zinc-blende InAs and InP NWs as a function of diameter (in Å).

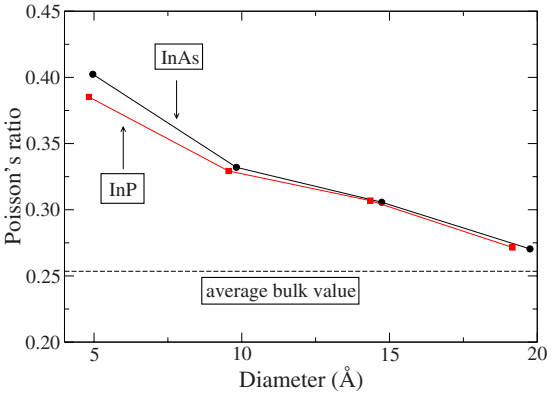

FIG. 4. (Color online) Calculated Poisson's ratios of the [111] zinc-blende InAs and InP NWs as a function of diameter (in Å). The horizontal dashed line represent the average Poisson's ratio of the bulk InAs and InP materials.

take the influence of the surface on the NWs Young's moduli as the difference between the effective Young's modulus for each NW and Young's modulus of the respective bulk material. The deviations from the bulk Young's modulus are dependent on the surface/volume ratio of the NWs, which for regular hexagonal prism NWs is $\approx 4.62/D$, where D is the wire diameter. We then propose to fit ΔY vs diameter by a function given by

$$Y_{NW}(D) = Y_0 + \frac{D_1}{D^n}, \tag{3}$$

where D_1, is a scale factor corresponding to the variation in the Young's modulus relative to the bulk value for a NW with a 1 Å diameter. D_1 and n are adjustable parameters. We assume that the bulk value would be obtained for NWs with diameters larger than 100 nm. These fits are shown in Fig. 3, with the fitted values for D_1 and n being −1.38 and 1.10 for InAs and −0.80 and 0.82 for InP, respectively. These values for D_1 and n can be slightly changed when the bulk limit is assumed to be different from 100 nm but it does not change the whole picture. To the best of our knowledge, there is no available experimental data for comparison. From Fig. 3 one can see that the influence of the surface will be significant for diameters shorter than 15 nm, with the deviations from the bulk values being more pronounced for the InP NWs. There is a great similarity in the general behavior of the diameter dependence of Young's modulus variation for the InAs and InP NWs. We would like to stress that the extrapolations to larger diameters in Fig. 3 should be considered carefully since the data set is restricted to a limited range of small diameters.

The lateral shrink or expansion of the NW diameters when subjected to external stress, the Poisson's ratio, can be calculated for the InAs and InP NWs, according to the following equation:

$$\frac{\Delta D}{D} = -\nu\epsilon. \tag{4}$$

As can be seen from Fig. 4, the Poisson's ratios for both NWs increase for decreasing diameters and have very similar

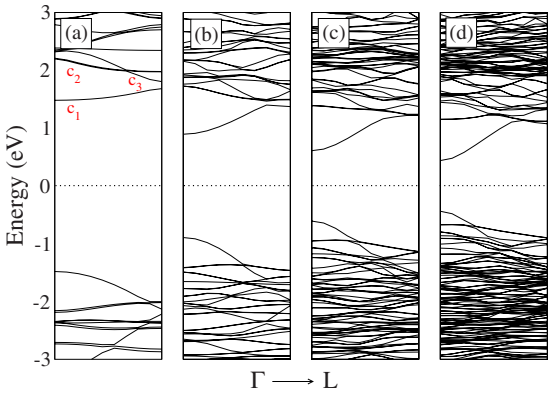

FIG. 5. (Color online) Calculated band structure for the [111] InAs nanowires with diameters of ≈ (a) 0.5, (b) 1.0, (c) 1.5, and (d) 2.0 nm. The Fermi energy is at 0 eV and is showed by the horizontal dashed line. The letters c_1, c_2, and c_3 in panel (a) indicate, in this order, the conduction-band minimum and two levels above in energy.

values, resembling the similarities between the InAs and InP bulk Poisson's ratios in Table II, with small differences appearing only at $D<10$ Å.

B. Electronic properties

The electronic structure of the InAs and InP NWs will be analyzed by taking into account [Eq. (1)] the diameter dependence and [Eq. (2)] the influence of external stress.

1. Diameter dependence

The lateral quantum confinement is well known to increase the energy separation between the valence and conduction levels of the NWs, increasing their band-gaps. This is shown in Fig. 5, for the studied InAs NWs. The band structures for the InP NWs are very similar and will not be shown here. Table III shows the calculated band-gap variations, ΔE_g. According to the simple quantum-mechanical particle in a box model,[62] it should be expected that the increase in the band-gap value would follow a $1/D^2$ behavior. However, deviations from this simple model have been reported for small diameter semiconductor NWs.[28,63,64] We

TABLE III. Calculated variations in the band-gaps relative to the bulk values, ΔE_g in eV, electron, m_e^*/m_0, and light-hole effective-mass (Ref. 65), m_{lh}^*/m_0 (m_0 is the free-electron mass), for the InAs and InP nanowires with different diameters, D.

D (nm)	InAs			InP		
	ΔE_g	m_e^*/m_0	m_{lh}^*/m_0	ΔE_g	m_e^*/m_0	m_{lh}^*/m_0
≃0.5	3.30			3.00		
≃1.0	2.12	0.277	0.198	1.87	0.489	0.245
≃1.5	1.56	0.153	0.125	1.32	0.244	0.183
≃2.0	1.22	0.106	0.092	1.00	0.182	0.133
∞ expt.[a]		0.023	0.025		0.079	0.089

[a]Reference 58.

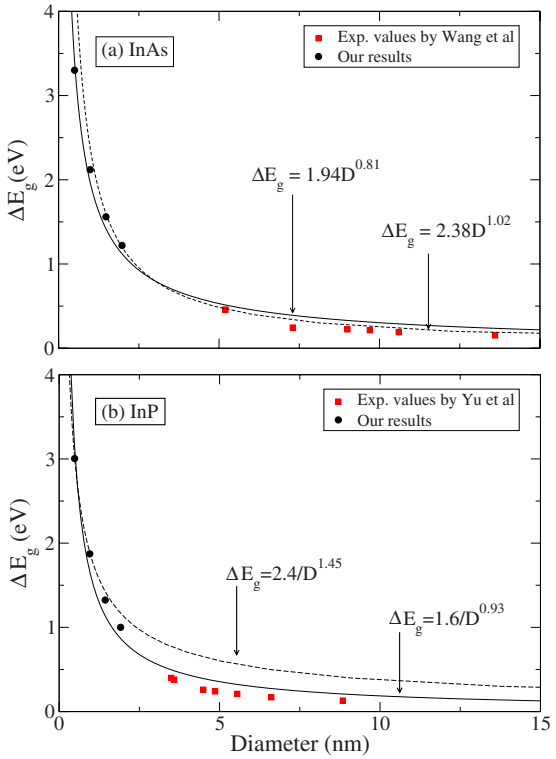

FIG. 6. (Color online) Variation in the band-gap, ΔE_g, for the InAs and InP NWs as a function of diameter, in nm. The solid lines are the results from our fits while the dashed lines correspond to similar fits presented in (a) Wang *et al.* (Ref. 64) and (b) Yu *et al.* (Ref. 63).

assume that the band-gaps of the InAs and InP NWs, $E_g^{\mathrm{NW}}(D)$, will vary according to the following formula:

$$E_g^{\mathrm{NW}}(D) = E_g^{bulk} + \frac{D_1}{D^{\alpha}}, \tag{5}$$

where E_g^{bulk} is the calculated bulk band-gap and D_1 is a scale factor corresponding to the variation in the band-gap for a NW with a diameter of 1 nm relative to the bulk value. The fit to this function is shown in Fig. 6, where we take into account the calculated $\Delta E_g(D)=E_g^{\mathrm{NW}}(D)-E_g^{bulk}$ values for the studied NWs, together with sets of experimental data for InAs (Ref. 64) and InP (Ref. 63) NWs. We also considered an asymptotic zero value to $\Delta E_g(D)$ at 100 nm. The increase in the band-gap occurs at rates which are lower than that given by $1/D^2$, with the α values in Eq. (5) for the InAs and InP NWs being 0.81 and 0.93, respectively. The D_1 values are 1.94 and 1.60 nm for InAs and InP NWs, respectively. The dashed curves in Figs. 6(a) and 6(b) correspond to the same kind of fit performed in previous works for InAs (Ref. 64) and InP (Ref. 63) NWs while the solid lines correspond to our fits. For the InAs NWs, it can be noted that both solid and dashed curves fit well the experimental and theoretical data. In the case of InP NWs, on the other hand, it is clearly seen that our fit gives a much better agreement with the experimental data, as compared to that by Yu *et al.*[63] We would like to stress that for the studied NWs, which have hexagonal cross sections, the definition of the diameter is not

obvious, as already stated. It happens because deviations from a cylindrical-like shape are enhanced when the edges/faces ratio is increased. So, the scaling behavior of the band-gap with diameter should not be expected to be so accurate for the thinner NWs.

Another evidence of the electronic structure dependence on the diameters of the InAs and InP NWs is given by the effective-masses. As is apparent from Fig. 5, the curvature of the conduction-band minimum (CBM) of the NWs diminishes when the diameter decreases. The electron and hole effective-masses for these NWs have been calculated and are shown in Table III. Although it is well known that LDA fails to accurately predict the effective-masses, the trends observed in this variation are expected to be correct and indicate that the increase in the surface/volume ratio will reduce the electron and hole mobility as the diameter decreases. It has a direct impact on the use of these NWs as active parts in nanoelectronic devices since it directly affects the carrier mobility. Even for the NWs with larger diameters, the calculated electron effective-masses are $\simeq 3.2$ times bigger than those for the bulk InAs and InP materials. This increase in the effective-masses with the narrowing of the NW diameters occurs due to a k dependence of the confinement effects on the electronic states, i.e., the shift on the conduction-band minimum at Γ is greater than those for the k vectors along the [111] direction. It is a consequence of the folding at Γ of the electronic states in directions other than that defined by the NW axis. Noteworthy is the fact that the hole effective-mass is lower than the corresponding electron effective-mass for a given NW, with the difference between them increasing with decreasing diameters.

Excepting the CBM level for the narrowest NW, the band-edge levels at the L point and Γ point will be different. For the VBM, two levels of different symmetry (one of them twofold degenerate) cross at k points which change with diameter, going from values close to Γ to values close to L as the diameter decreases. The twofold-degenerate level will be the VBM level at L point. For the CBM, there is an anticrossing between two highly dispersive levels which have the same symmetry, c_1 and c_3, and crossings involving these two levels and a twofold-degenerate level of different symmetry, c_2 (c_1, c_2, and c_3 are defined in Fig. 5). These crossings and anticrossings close to the L point change the character of the CBM level for different diameters. For the NW with the largest diameter, the CBM at the L point is given by the nondegenerate level which has higher energy at Γ, c_3. For the NW with diameter ≈ 1.5 nm, a quasi-degeneracy between the c_2 and c_3 levels seems to occur. For the 1.0 nm NW, the c_3 level is again the CBM at L, and for the 0.5 diameter NW, it will be given by the c_1 level, which is the CBM at the Γ point for all NW diameters.

Another electronic quantity that can be measured experimentally is the work function, i.e., the energy necessary to extract an electron from the material. We calculate the electronic work function, Φ, of the InAs and InP NWs according to the following formula:

$$\Phi = V_{vac} - E_f, \tag{6}$$

where V_{vac} is the electrostatic potential at the vacuum region and E_f is the electronic Fermi energy, which we define as the energy at the middle of the band-gap. The calculated work functions for the studied NWs are shown in Table IV. It can be seen that the work function increases monotonically with increasing diameter, which is in accordance with experimental results for InAs quantum dots.[66] The decreasing ratio of the work function with decreasing diameter is almost material independent, and will be greater for narrower NWs. It indicates that the variation in the work function is mainly dependent on the surface/volume ratio. From these values, one can see that electrons will be more easily detached as thinner the NWs.

TABLE IV. Calculated work function, Φ, as a function of diameter for the InAs and InP NWs.

D (nm)	Φ (eV)	
	InAs	InP
$\simeq 0.5$	4.36	4.24
$\simeq 1.0$	4.49	4.36
$\simeq 1.5$	4.59	4.45
$\simeq 2.0$	4.68	4.52

2. Stress dependence

The electronic levels in NWs can vary due to effects other than those coming from quantum confinement, e.g., lattice distortions due to phonon states. This is crucial when electronic transport is considered. Bardeen and Shockley[67] first showed that long-wavelength phonon states affect the band-edge levels, and consequently the electronic transport, and that these effects can be well reproduced by homogeneous deformations of the material system. The influence of these lattice deformations on the electronic states can be described by effective potentials called deformation potentials. The deformation potentials will depend on (i) the space group of the material system, (ii) the wave vector, and (iii) symmetry of the electronic state in question.[68]

We have determined the volume deformation potential for CBM and valence-band maximum (VBM), $a_V^i = \partial E_i / \partial \ln(V)$, at the Γ point for the bulk InP material, where E_i is the eigenvalue of the electronic state i and V is the volume of the material system. From these two deformation potentials, one can define the band-gap deformation potential as $a_V^g = a_V^{\mathrm{CBM}} - a_V^{\mathrm{VBM}}$. The results for a_V^g, a_V^{CBM}, and a_V^{VBM} are -5.50, -15.47, and -9.97 eV, respectively. It should be regarded that the only measurable of these deformation potentials is a_V^g. Different calculations can give different values for the a_V^{CBM} and a_V^{VBM} since there is no absolute reference in terms of which these values could be obtained. Actually, theoretical values ranging from -3.4 to -21 eV have been obtained for the a_V^{CBM}.[9] Our results for the band-gap deformation potentials are in good agreement with Wei and Zunger,[69] -5.30 eV, and Van de Walle,[70] -6.31 eV.

For NWs, there is only one direction where the translational symmetry is preserved. Thus, the deformation potential associated with an electronic level i in NWs will be given

TABLE V. Calculated band-gap, a^g, conduction, a^{CBM}, and valence, a^{VBM}, deformation potentials, for the InAs and InP nanowires with different diameters, D. The values are given in eV.

D (nm)	InAs			InP		
	a^{VBM}	a^{CBM}	a^g	a^{VBM}	a^{CBM}	a^g
≃0.5	−4.03	−6.57	−2.54	−4.26	−6.98	−2.72
≃1.0	−6.61	−7.57	−0.96	−6.72	−8.07	−1.35
≃1.5	−8.09	−7.74	0.35	−8.28	−8.45	−0.17
≃2.0	−8.98	−7.86	1.12	−9.15	−8.66	0.49

by $\partial E_i/\partial \epsilon$, where ϵ means the axial strain. This quantity has already been determined for [110] and [111] Si NWs by Leu *et al.*[45] The calculated band-gap, CBM and VBM deformation potentials for the InAs and InP NWs with different diameters are shown in Table V. These deformation potentials are calculated using both CBM and VBM eigenvalues at the Γ point. It can be seen from the data in Table V that the CBM and VBM deformation potentials decrease as the NW diameter decreases, which shows that the band-edges will be less affected by external stress as the NW turns thinner. Further, the variation in VBM deformation potential with diameter is greater than that for the CBM in both wires. For the thicker wires, the VBM deformation potentials are greater than the CBM ones while for the thinner wires this relationship is inverted. It leads to a sign change in the band-gap deformation potential with the NW diameter. For the thicker wires, the band-gap increases (decreases) for tensile (compressive) stress whereas for the thinner wires the band-gap decreases (increases) for tensile (compressive) stress. The lowest absolute values for the band-gap deformation potentials are obtained for the NWs with diameters around 1.5 nm. These are the NWs which have band-gaps less sensitive to external strain and are close to the threshold diameter where an inversion in the band-gap behavior with stress takes place.

Actually, the strain along the NW axis also introduces deformations in the NW diameters, according to the Poisson's ratio. The effect of these radial deformations on the electronic levels will appear as an additional confinement effect and cannot be associated to deformation potentials since there is no periodicity along the radial direction. The influence of the strain on the electronic levels can be written as

$$L_0\left(\frac{dE_i}{dL}\right)_{L=L_0} = L_0\left(\frac{\partial E_i}{\partial L}\right)_{L=L_0} + L_0\left(\frac{\partial E_i}{\partial D}\frac{\partial D}{\partial L}\right)_{L=L_0} = \frac{\partial E_i}{\partial \epsilon} - \nu D\frac{\partial E_i}{\partial D}. \quad (7)$$

The first term on the right side of Eq. (7) represents the axial deformation potentials while the second term gives the shift on the electronic level E_i due to the variation in the NW diameter, which appears as a quantum confinement effect and is directly proportional to the Poisson's ratio ν. We have separately estimated the effects of the two terms on the right-hand side of Eq. (7) for the ≈0.5 nm diameter InP NW by considering configurations in which (i) the resulting axial deformation is such as for the NW deformed in 4% in its lattice constant but with the diameter kept the same as for the unstrained NW and (ii) the reduction in the diameter is the same as for the NW deformed in 4% in its lattice constant but with the axial length kept as for the NW at zero axial strain. The shifts in the band-edge eigenvalues, ΔE^{VBM} and ΔE^{CBM}, due to the axial and radial deformations are ΔE^{VBM}=−0.154 and −0.020 eV, and ΔE^{CBM}=−0.327 and 0.010 eV, respectively. It can be seen that the shift in the eigenvalues at the Γ point due only to axial deformations, which can be interpreted as a rigid diameter axial deformation potential, are 7.7 and 50 times greater for the VBM and CBM, respectively, than the shift in the eigenvalues due only to the radial confinement. The magnitude of this additional radial confinement energy shift is directly proportional to the Poisson's ratio, as noted before.

The band structures of the InAs NWs for axial strains from −4% to 4% of the axial lattice constant are shown in Fig. 7. The band structures for the InP NWs are similar and not shown here. Axial strains act differently on the various levels appearing in the band structure, depending on the spatial decomposition of the charge densities associated with the levels. Levels with greater components along the axial direction will be more affected by the axial strain, although levels with greater charge densities in directions perpendicular to the NW axis will also be affected, due to the radial deformations of the NWs following the axial strains. Table VI shows the s, $p_\perp$, and $p_\parallel$ components of selected levels close to the band-gap at the Γ and L points for the thinnest NWs at a 0.04 strain. The symbols $p_\parallel$ and $p_\perp$ stand for the parallel and perpendicular components of p-like orbitals with respect to the NW axis.

As can be seen from Table VI, the VBM level has greater components along the NW axis while the CBM has mainly s character. It implies that the VBM levels would be more affected by the axial strain. This should appear as greater a^{VBM} than a^{CBM} values. Actually, this is observed for the thicker NWs. However, as the NWs turn thinner, larger Poisson's and surface/volume ratios make the confinement effects on levels with greater s and $p_\perp$ components more evident. Since the CBM is mainly s character, the greater radial deformations and lower diameters of the thinner NWs will make the a^{CBM} values higher than a^{VBM} ones. Figure 7 shows that the dispersion of the CBM band do not to change significantly with strain for the two thicker NWs but present evident variation for the two thinner ones. The VBM level does not change its main contributions at the Brillouin-zone end points. On the other hand, the twofold-degenerate VBM-1 level does change its contributions, having greater $p_\perp$ and $p_\parallel$ characters at Γ and L, respectively, for the thinnest diameter NWs. Whereas the VBM and CBM levels maintain their characters for all studied diameters, the VBM-1 does not. Actually, as the diameter is increased from 0.5 to 2.0 nm, the VBM-1 gradually changes its main character from $p_\perp$ to $p_\parallel$ at Γ and from $p_\parallel$ to $p_\perp$ at L. This change in the VBM-1 character as a function of diameter explains why the VBM and VBM-1 eigenvalues turn closer in energy as the diameter is increased. From Fig. 7, one can see that the relative energy difference between the VBM and VBM-1 changes with

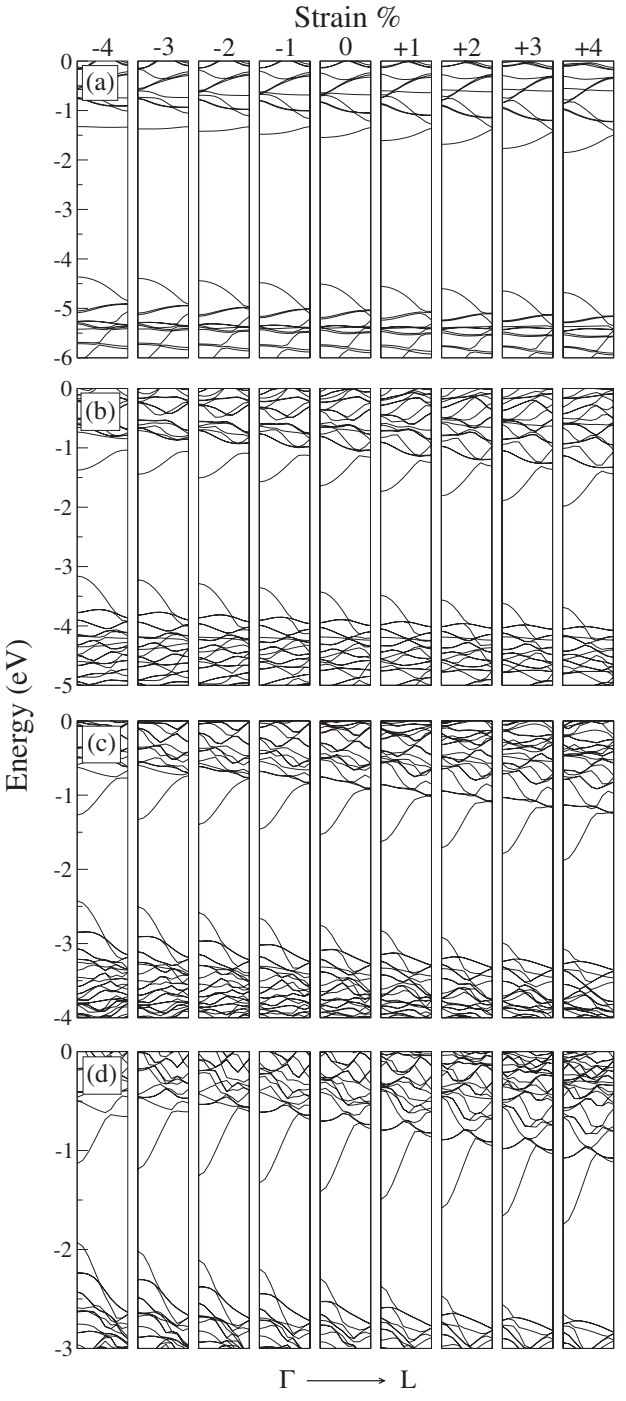

FIG. 7. Calculated band structures for InAs NWs with diameters of ≈ (a) 0.5, (b) 1.0, (c) 1.5, and (d) 2.0, as a function of strain, which corresponding to axial distortions from −4% to +4% of the NW equilibrium lattice constant.

strain. For tensile (compressive) stress, these levels shift to lower (higher) energies with a ratio that depends directly on the $p_{\parallel}$ content of the level, which is higher for the VBM. Then, the shifts in the VBM will be greater than those in the VBM-1 and the levels will approach (separate) each other in energy at the Γ point for tensile (compressive) strains. This last trend combined with the relative energy position at zero strain leads to the observed structure of the levels at the top of the valence-band for the studied NWs, as seen in Fig. 7.

TABLE VI. Calculated charge density decomposition for levels of the InAs NW close to the band-gap. The VBM-1, VBM, and CBM labels are assigned according to the level ordering appearing in the band structure for the narrowest NW at −4% strain (upper left panel in Fig. 7).

	Γ			*L*		
	s	$p_{\parallel}$	$p_{\perp}$	*s*	$p_{\parallel}$	$p_{\perp}$
VBM-1	0.060	0.113	0.400	0.033	0.310	0.025
VBM	0.047	0.508	0.022	0.057	0.475	0.042
CBM	0.472	0.017	0.032	0.346	0.066	0.019

The effective-masses will also be affected by strain. This additional variation in the effective-mass is related to a *k* dependence of the strain effects on the band-edge levels. This *k* dependence can also be analyzed by taking into account the changes in the level decomposition in *s*, $p_{\perp}$, and $p_{\parallel}$ contributions. As noted above, the CBM level is more affected in the thinner NWs. From Table VI it can be seen that the CBM has greater $p_{\parallel}$ contributions at *L* than at Γ. Thus, the variation in the CBM with axial stress will be greater at *L* than at Γ, which will change the CBM dispersion and effective-mass values, as can be seen from Figs. 7(a) and 7(b). As the NWs turn thicker, this effect is less manifest. It could be explored for nanoelectromechanical sensors, with the mobility changing with stress. This *k*-dependent behavior of the CBM with strain lead even to a direct-indirect transition of the band-gap, and to very high values of the electron effective-mass. This band-gap transition is observed to occur for the thinnest NWs at ≈−0.03 strain. Another direct to indirect band-gap transition is suggested to occur for thicker NWs at tensile strains, as is evident from the evolution of the levels close to the valence-band maximum in Fig. 7(d). Noteworthy is the fact that for the studied thin InAs and InP NWs, the calculated hole effective-masses are seen to be lower than the respective electron effective-masses.

IV. CONCLUSIONS

In summary, we performed first-principles calculations to study the mechanical, structural, and electronic properties of [111] zinc-blende InAs and InP NWs. We determined the behavior of the axial lattice constants, Young's modulus, and Poisson's ratio of both NWs as a function of diameter and showed that they differ from their respective bulk values. The lattice constants and Young's modulus decrease while the Poisson's ratio increases with decreasing diameter. The increase in the band-gaps with lateral confinement is shown to differ from the $1/D^2$ behavior predicted by simple quantum-mechanical particle in a box model, with greater deviations for the smaller diameter NWs. The work functions of both NWs are seen to decrease with decreasing diameters. The effective-masses are determined to increase with decreasing diameters, as a consequence of *k*-dependent shifts in the band-edge eigenvalues, and has no dependence on any surface related scattering mechanism. The band-gap deformation potentials are determined and seen to vary nonmono-

tonically with diameter, from positive to negative values as the diameter decreases. The variation in the band-edges and effective-masses with strain is analyzed in terms of a charge decomposition along directions parallel and perpendicular to the NW axis, and very high electron effective-mass values as well as a direct to indirect band-gap transition is observed to occur for the thinnest NWs at compressive strains. Direct to indirect band-gap transition occurring simultaneously with transition from low to high hole effective-mass regimes are suggested to occur at tensile strains for larger diameter NWs.

ACKNOWLEDGMENTS

This work has been supported by the Brazilian agencies CAPES and CNPq. The calculations were performed at the Centro Nacional de Processamento de Alto Desempenho, CENAPAD/Campinas.

[1] A. I. Persson, M. T. Bjork, S. Jeppeesen, J. B. Wagner, L. R. Wallenberg, and L. Samuelson, Nano Lett. **6**, 403 (2006).
[2] X. F. Duan, Y. Huang, Y. Cui, J. Wang, and C. M. Lieber, Nature (London) **409**, 66 (2001).
[3] Y. Huang, X. F. Duan, Y. Cui, L. J. Lauhon, K.-H. Kim, and C. M. Lieber, Science **294**, 1313 (2001).
[4] Y. Cui, Q. Q. Wei, H. K. Park, and C. M. Lieber, Science **293**, 1289 (2001).
[5] M. H. Huang, S. Mao, H. Feick, H. Yan, Y. Wu, H. Kind, E. Weber, R. Russo, and P. Yang, Science **292**, 1897 (2001).
[6] F. Zhang, V. H. Crespi, and P. Zhang, Phys. Rev. Lett. **102**, 156401 (2009).
[7] Z. L. Wang and J. Song, Science **312**, 242 (2006).
[8] X. Wang, J. Song, J. Liu, and Z. L. Wang, Science **316**, 102 (2007).
[9] I. Vurgaftman, J. R. Meyer, and L. R. Ram-Mohan, J. Appl. Phys. **89**, 5815 (2001).
[10] C. Thelander, M. T. Björk, M. W. Larsson, A. E. Hansen, L. R. Wallenberg, and L. Samuelson, Solid State Commun. **131**, 573 (2004); C. Thelander, C. Rehnstedt, L. E. Fröberg, E. Lind, T. Mårtensson, P. Caroff, T. Löwgren, B. J. Ohlsson, L. Samuelson, and L.-E. Wernersson, IEEE Trans. Electron Devices **55**, 3030 (2008).
[11] O. Karlström, A. Wacker, K. Nilsson, G. Astromskas, S. Roddaro, L. Samuelson, and L.-E. Wernersson, Nanotechnology **19**, 435201 (2008).
[12] B. S. Sørensen, M. Aagesen, C. B. Sørensen, P. E. Lindelof, K. L. Martinez, and J. Nygård, Appl. Phys. Lett. **92**, 012119 (2008).
[13] S. A. Dayeh, E. T. Yu, and D. Wang, Small **5**, 77 (2009).
[14] A. C. Ford, J. C. Ho, Y.-L. Chueh, Y.-C. Tseng, Z. Fan, J. Guo, J. Bokor, and A. Javey, Nano Lett. **9**, 360 (2009).
[15] D. B. Suyatin, C. Thelander, M. T. Björk, I. Maximov, and L. Samuelson, Nanotechnology **18**, 105307 (2007).
[16] K. Tomioka, J. Motohisa, S. Hara, and T. Fukui, Nano Lett. **8**, 3475 (2008).
[17] Q. Hang, F. Wang, P. D. Carpenter, D. Zemlyanov, D. Zakharov, E. A. Stach, W. E. Buhro, and D. B. Janes, Nano Lett. **8**, 49 (2008).
[18] M. Mattila, T. Hakkarainen, M. Mulot, and H. Lipsanen, Nanotechnology **17**, 1580 (2006).
[19] A. Mishra, L. V. Titova, T. B. Hoang, H. E. Jackson, L. M. Smith, J. M. Yarrison-Rice, Y. Kim, H. J. Joyce, Q. Gao, H. H. Tan, and C. Jagadish, Appl. Phys. Lett. **91**, 263104 (2007).
[20] L. K. van Vugt, S. J. Veen, E. P. A. M. Bakkers, A. L. Roest, and D. Vanmaekelbergh, J. Am. Chem. Soc. **127**, 12357 (2005).
[21] R. E. Algra, M. A. Verheijen, M. T. Borgström, L.-F. Femeasurablemink, W. J. P. van Enckevort, E. Vlieg, and E. P. A. M. Bakkers, Nature (London) **456**, 369 (2008).
[22] D. M. Cornet, V. G. M. Mazzetti, and R. R. LaPierre, Appl. Phys. Lett. **90**, 013116 (2007).
[23] M. T. Borgström, E. Norberg, P. Wickert, H. A. Nilsson, J. Trägårdh, K. A. Dick, G. Statkute, P. Ramvall, K. Deppert, and L. Samuelson, Nanotechnology **19**, 445602 (2008).
[24] M. S. Gudiksen, J. Wang, and C. M. Lieber, J. Phys. Chem. B **106**, 4036 (2002).
[25] M. Moewe, L. C. Chuang, V. G. Dubrovskii, and C. Chang-Hasnain, J. Appl. Phys. **104**, 044313 (2008).
[26] M. Galicka, M. Bukala, R. Buczko, and P. Kacman, J. Phys.: Condens. Matter **20**, 454226 (2008).
[27] M. P. Persson and H. Q. Xu, Phys. Rev. B **73**, 125346 (2006).
[28] T. M. Schmidt, R. H. Miwa, P. Venezuela, and A. Fazzio, Phys. Rev. B **72**, 193404 (2005).
[29] M. D. Moreira, P. Venezuela, and T. M. Schmidt, Nanotechnology **19**, 065203 (2008).
[30] T. Akiyama, K. Nakamura, and T. Ito, Phys. Rev. B **73**, 235308 (2006).
[31] M. M. G. Alemany, X. Huang, M. L. Tiago, L. J. Gallego, and J. R. Chelikowsky, Nano Lett. **7**, 1878 (2007).
[32] Y. Zhang, Y.-H. Wen, J.-C. Zheng, and Z.-Z. Zhu, Appl. Phys. Lett. **94**, 113114 (2009).
[33] M. D. Lyons, R. M. Ryan, A. M. Morris, and J. D. Holmes, Nano Lett. **2**, 811 (2002).
[34] L. Huang, N. Lu, J.-A. Yan, M. Y. Chou, C.-Z. Wang, and K.-M. Ho, J. Phys. Chem. C **112**, 15680 (2008).
[35] A. J. Lu, R. Q. Zhang, and S. T. Lee, Appl. Phys. Lett. **91**, 263107 (2007).
[36] B. M. Haugerud, L. A. Bosworth, and R. E. Belford, J. Appl. Phys. **94**, 4102 (2003).
[37] H. W. Seo, S. Y. Bae, J. Park, H. N. Yang, K. S. Park, and S. Kim, J. Chem. Phys. **116**, 9492 (2002).
[38] M. Luisier, A. Schenk, W. Fichtner, and G. Klimeck, Phys. Rev. B **74**, 205323 (2006).
[39] F. Bogár, J. W. Mintmire, F. Bartha, T. Mezö, and C. Van Alzenoy, Phys. Rev. B **72**, 085452 (2005).
[40] M. Verissimo-Alves, B. Koiller, H. Chacham and R. B. Capaz, Phys. Rev. B **67**, 161401(R) (2003).
[41] X. D. Bai, P. X. Gao, Z. L. Wang, and E. G. Wang, Appl. Phys. Lett. **82**, 4806 (2003).
[42] H. Ni and X. D. Li, Nanotechnology **17**, 3591 (2006).
[43] C. Q. Chen, Y. Shi, Y. S. Zhang, J. Zhu, and Y. J. Yan, Phys. Rev. Lett. **96**, 075505 (2006).

[44] B. Wang, J. Zhao, J. Jia, D. Shi, J. Wan, and G. Wang, Appl. Phys. Lett. **93**, 021918 (2008).
[45] P. W. Leu, A. Svizhenko, and K. Cho, Phys. Rev. B **77**, 235305 (2008).
[46] S. Cuenot, C. Fretigny, S. Demoustier-Champagne, and B. Nysten, Phys. Rev. B **69**, 165410 (2004).
[47] B. Wu, A. Heidelberg, and J. J. Boland, Nature Mater. **4**, 525 (2005).
[48] G. Wang and X. Li, Appl. Phys. Lett. **91**, 231912 (2007).
[49] R. E. Miller and V. B. Shenoy, Nanotechnology **11**, 139 (2000).
[50] G. Y. Jing, H. L. Duan, X. M. Sun, Z. S. Zhang, J. Xu, Y. D. Li, J. X. Wang, and D. P. Yu, Phys. Rev. B **73**, 235409 (2006)
[51] H. Liang, M. Upmanyu, and H. Huang, Phys. Rev. B **71**, 241403(R) (2005).
[52] G. Kresse and J. Hafner, Phys. Rev. B **47**, 558 (1993); G. Kresse and J. Furthmüller, *ibid.* **54**, 11169 (1996).
[53] D. M. Ceperley, and B. J. Alder, Phys. Rev. Lett. **45**, 566 (1980).
[54] J. P. Perdew and A. Zunger, Phys. Rev. B **23**, 5048 (1981).
[55] P. E. Blöchl, Phys. Rev. B **50**, 17953 (1994).
[56] H. J. Monkhorst and J. D. Pack, Phys. Rev. B **13**, 5188 (1976).
[57] F. D. Murnaghan, Proc. Natl. Acad. Sci. U.S.A. **30**, 244 (1944).
[58] *Semiconductors, Physics of Group IV Elements and III-V Compounds*, Landolt-Börnstein, New Series, Group III Vol. 17, edited by O. Madelung, M. Schulz, and H. Weiss (Springer-Verlag, New York, 1982).
[59] S. W. Ellaway and D. A. Faux, J. Appl. Phys. **92**, 3027 (2002).
[60] S. Adachi, *Physical Properties of III-V Semiconductors Compounds* (John-Wiley & Sons, New York, 1992).
[61] Pseudo-H atoms have fractional charges choosen to mimic the charges at bondings bulk systems. For example, the charges for pseudo-H atoms bonded to In (As) atoms should be 1.25 (0.75) instead of 1.0, as for real H atoms.
[62] S. Gasiorowicz, *Quantum Physics* (John Wiley & Sons, Hoboken, 2003).
[63] H. Yu, J. Li, R. A. Loomis, L.-W. Wang, and W. E. Buhro, Nature Mater. **2**, 517 (2003).
[64] F. Wang, H. Yu, S. Jeong, J. M. Pietryga, J. A. Hollingsworth, P. C. Gibbons, and W. E. Buhro, ACS Nano **2**, 1903 (2008).
[65] We relate the effective-mass of the NWs' valence-band maximum to the bulk light-hole effective-mass due to the greater dispersion of the VBM.
[66] T. Yamauchi, M. Tabuchi, and A. Nakamura, Appl. Phys. Lett. **84**, 3834 (2004).
[67] J. Bardeen and W. Shockley, Phys. Rev. **80**, 72 (1950).
[68] P. Y. Yu and M. Cardona, *Fundamentals of Semiconductors* (Springer, New York, 2005).
[69] S.-H. Wei and A. Zunger, Phys. Rev. B **60**, 5404 (1999).
[70] C. G. Van de Walle, Phys. Rev. B **39**, 1871 (1989).